Elliptical monogenic representation of color images and local frequency analysis

Raphaël Soulard, Philippe Carré

ELLIPTICAL MONOGENIC REPRESENTATION OF COLOR IMAGES AND LOCAL FREQUENCY ANALYSIS

Raphaël Soulard and Philippe Carré

XLIM-SIC Department UMR CNRS 7252, University of Poitiers, France.

ABSTRACT

We define a new color extension for the monogenic representation of images by using an elliptical tri-valued oscillation model jointly with the vector structure tensor formalism. The proposed method provides a rich local colorimetric and geometric analysis, in particular a color phase concept, which can be computed by a numerically stable algorithm. This representation is finally used to estimate the local frequency of color images.

Index Terms— wavelet transform, color, analytic signal, monogenic signal, monogenic wavelets, local frequency

1. THE MONOGENIC REPRESENTATION

As a 2D extension of the *analytic signal*, the monogenic signal [1] provides a 2D AM/FM representation of greyscale images. Thanks to its rotation invariance property and its underlying *signal shape* analysis; the monogenic representation has been used for numerous image applications, including analysis of textures [2], contours [1], motion or stereo disparity [3, 4]; segmentation [5, 6] *etc.*

Given a 2D real signal $s(\boldsymbol{x})$, the associated monogenic signal $s_M(\boldsymbol{x})$ is the following 3-vector valued signal:

$$s_M(\boldsymbol{x}) = \begin{bmatrix} s(\boldsymbol{x}) \\ \Re\{\mathcal{R}s(\boldsymbol{x})\} \\ \Im\{\mathcal{R}s(\boldsymbol{x})\} \end{bmatrix} = \begin{bmatrix} A(\boldsymbol{x})\cos\varphi(\boldsymbol{x}) \\ A(\boldsymbol{x})\sin\varphi(\boldsymbol{x})\cos\theta(\boldsymbol{x}) \\ A(\boldsymbol{x})\sin\varphi(\boldsymbol{x})\sin\theta(\boldsymbol{x}) \end{bmatrix} \quad (1)$$

where $\mathcal{R}s$ is the complex-valued Riesz transform of s:

$$\{\mathcal{R}s\}(\boldsymbol{x}) = p.v.\!\int \frac{\tau_1+\mathbf{j}\tau_2}{2\pi\|\boldsymbol{\tau}\|^3}\, s(\boldsymbol{x}-\boldsymbol{\tau})\, d\boldsymbol{\tau} \;\overset{\mathcal{F}}{\longleftrightarrow}\; \frac{\omega_2-\mathbf{j}\omega_1}{\|\boldsymbol{\omega}\|}\,\hat{s}(\boldsymbol{\omega}) \quad (2)$$

(see also [7, 8]). The monogenic features are given by the spherical coordinates of s_M:

$$\begin{array}{ll} \text{Amplitude:} & A = \sqrt{s^2+|\mathcal{R}s|^2} \\ \text{Orientation:} & \theta = \arg\{\mathcal{R}s\} \in [-\pi;\pi[\\ \text{1D Phase:} & \varphi = \arg\{s+\mathbf{j}|\mathcal{R}s|\} \in [0;\pi] \end{array} \quad (3)$$

This representation is equivalent to the pointwise estimation of the underlying *plane wave* that locally resembles the signal. The signal is modelled by an "A-strong" plane wave with orientation θ, and phase-shifted according to φ - which explicitely indicates if the structure is rather a *line* or an *edge*.

The goal of this paper is to study the generalization of this tool for color images. Analyzing color data is essential for a lot of applications. However, due to a lack of definition in multi-dimensional signal processing, color images are most often handled by a suboptimal use of scalar tools, either by only considering luminance, or by working separately on every color channel ("marginal" scheme [9]). Note that a color monogenic signal is defined in [10], by generalizing the Cauchy-Riemann equations within Geometric algebra. However, we showed in [11] that this definition does not provide satisfactory physical interpretation of the obtained features. To go one step further, this paper handles the issue from the physical point of view.

We first define the 1D color elliptical model in section 2 in order to well understand what a "color oscillation" is. Then we extend it to our 2D color monogenic representation using the structure tensor formalism in section 3; and finally exploit it to estimate local frequency of color images in section 4.

2. THE COLOR 1D OSCILLATION

This section aims at redefining the classical *amplitude* and *phase* concepts for color signals. Our starting point is the sinusoidal signal model, building block of the Fourier analysis. It is well known that a Fourier coefficient is made of an amplitude and a phase value, directly giving the two parameters of a sinusoidal oscillation. We must then define what a *color oscillation* is.

Regarding the numerous generalized Fourier transforms in the mathematical literature *e.g.* [12, 13]; it seems reasonable to us to consider independent Fourier analyses at each color channel in the first place. Therefore, our proposition is to define the *color oscillation* by:

$$\mathbf{a}(t) = \begin{bmatrix} a^{\mathsf{R}}(t) \\ a^{\mathsf{G}}(t) \\ a^{\mathsf{B}}(t) \end{bmatrix} = \begin{bmatrix} A^{\mathsf{R}}\cos(\omega t+\varphi^{\mathsf{R}}) \\ A^{\mathsf{G}}\cos(\omega t+\varphi^{\mathsf{G}}) \\ A^{\mathsf{B}}\cos(\omega t+\varphi^{\mathsf{B}}) \end{bmatrix} \quad (4)$$

Parameters of $\mathbf{a}$ are directly obtained from separated Fourier analyses to form the complex valued 3-vector

$$\hat{\mathbf{a}} = \left[\, A^{\mathsf{R}}e^{\mathbf{j}\varphi^{\mathsf{R}}} \;\; A^{\mathsf{G}}e^{\mathbf{j}\varphi^{\mathsf{G}}} \;\; A^{\mathsf{B}}e^{\mathbf{j}\varphi^{\mathsf{B}}} \,\right]^{\mathsf{T}} \quad (5)$$

The problem is that those parameters do not allow any intuitive interpretation of how the oscillation is *modulated* by them. This is why a *non-marginal* construction must be carried out by some proper *conversion* of the 3 amplitudes and 3 phases into clearly identified geometric and colorimetric features. In particular, we may prefer to have an unique amplitude, and a physical color phase concept.

To this end, we must view $\mathbf{a}(t)$ like a point-trajectory (a "color path") within the 3D color space. Figures 1a and 1b show an example of *color sinusoid*, and its representation in the color space as a point-trajectory. We also plot the corresponding 2D wave in the image world 1d, which will be treated later.

What follows is based on the work in [14] that analyzes trajectories of particles in the field of seismology, which is perfectly analogous to our point. We here use it while adding the "color" concept.

It can be verified [14] that $\mathbf{a}(t)$ draws an *ellipse* within the color space - as illustrated on figures 1a and 1b with arbitrary values of amplitudes and phases. The *amplitude* concept can intuitively by

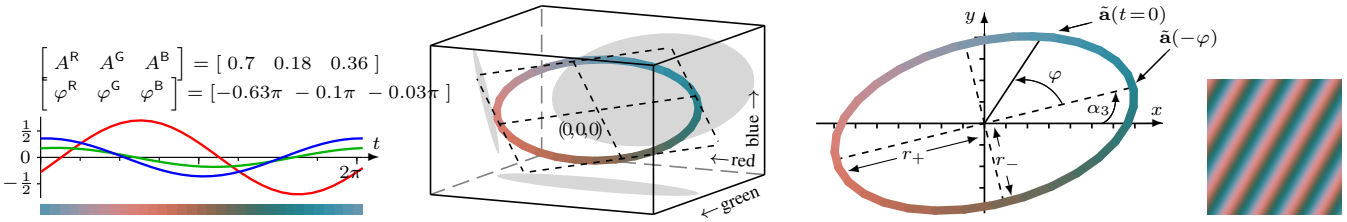

(a) 1D color sinusoid $\mathbf{a}(t)$ (b) Trajectory of $\mathbf{a}(t)$ in RGB space (c) Ellipse $\tilde{\mathbf{a}}(t)$ in the x-y plane (d) 2D atom

Fig. 1. Color sinusoidal oscillation. Colors of $\mathbf{a}(t)$ are generated by centering around middle grey and normalizing.

extended in the color case to the ellipse's *size*. The *phase* concept can also be handled, by defining it as the time-relative position of the oscillation's *maximum*. In the general case, the ellipse's *apogees* can be viewed like the sinusoid's *maxima*. So the phase φ can be defined by the time-relative position of the ellipse's apogee, as illustrated in figure 1c. The remaining ellipse parameters are expected to convey colorimetric information.

Let us now give the formulae to calculate the whole elliptical model, from the 6 original parameters A^{R}, A^{G}, A^{B}, φ^{R}, φ^{G} and φ^{B}.

First, $\mathbf{a}(t)$ admits the following normal vector:

$$\mathbf{n} = \begin{bmatrix} A^{\mathsf{G}}A^{\mathsf{B}}\sin(\varphi^{\mathsf{G}}-\varphi^{\mathsf{B}}) \\ A^{\mathsf{B}}A^{\mathsf{R}}\sin(\varphi^{\mathsf{B}}-\varphi^{\mathsf{R}}) \\ A^{\mathsf{R}}A^{\mathsf{G}}\sin(\varphi^{\mathsf{R}}-\varphi^{\mathsf{G}}) \end{bmatrix} = \|\mathbf{n}\| \begin{bmatrix} \sin\alpha_1 \sin\alpha_2 \\ -\cos\alpha_1 \sin\alpha_2 \\ \cos\alpha_2 \end{bmatrix} \quad (6)$$

This *color plane* (dotted lines in figure 1b) is parametrized by the two angles α_1 and α_2.

Let us now consider ellipse's size. The largest and smallest radius (a.k.a semi-major and semi-minor axes) r_+ and r_- are illustrated on figure 1c. They can be considered through two equivalent quantities, *amplitude* A and *linearity* λ:

$$A = \sqrt{(A^{\mathsf{R}})^2+(A^{\mathsf{G}})^2+(A^{\mathsf{B}})^2} = \sqrt{r_+^2+r_-^2} \quad (7)$$

$$\lambda = \sqrt{1-4\frac{\|\mathbf{n}\|^2}{A^4}} = \frac{r_+^2-r_-^2}{r_+^2+r_-^2} \quad (8)$$

The ellipse's position needs one more angle to be fully described: the angle α_3 (see fig. 1c). Its calculus is joint to this of the phase φ:

$$\alpha_3 = (\arg(\tilde{a}_1+\tilde{a}_2)-\arg(\tilde{a}_1-\tilde{a}_2))/2 \quad (9)$$

$$\varphi = (\arg(\tilde{a}_1+\tilde{a}_2)+\arg(\tilde{a}_1-\tilde{a}_2))/2 \quad (10)$$

and is based on the following rotation:

$$\begin{bmatrix} \tilde{a}_1 \\ \tilde{a}_2 \\ 0 \end{bmatrix} = \begin{bmatrix} \cos\alpha_1 & \sin\alpha_1 & 0 \\ -\cos\alpha_2\sin\alpha_1 & \cos\alpha_2\cos\alpha_1 & \sin\alpha_2 \\ \sin\alpha_1\sin\alpha_2 & -\cos\alpha_1\sin\alpha_2 & \cos\alpha_2 \end{bmatrix} \begin{bmatrix} A^{\mathsf{R}}e^{\mathbf{j}\varphi^{\mathsf{R}}} \\ A^{\mathsf{G}}e^{\mathbf{j}\varphi^{\mathsf{G}}} \\ A^{\mathsf{B}}e^{\mathbf{j}\varphi^{\mathsf{B}}} \end{bmatrix} \quad (11)$$

The phase φ is such that $\mathbf{a}(-\varphi)$ coincides with the ellipse's apogee: $\|\mathbf{a}(-\varphi)\| = r_+$.

We refer the reader to [14] for a detailed explanation, as well as for the reverse calculus to retrieve the 3 independent Fourier coefficients.

Eventually, we have converted 3 independent Fourier analyses into intuitive amplitude and phase data completed by 4 colorimetric features λ, α_1, α_2 and α_3. Let us now put this into the 2D monogenic framework.

3. ELLIPTICAL MONOGENIC REPRESENTATION

According to the *monogenic* formalism, the signal to analyse must be combined with its Riesz transform ("RT"). In order to better handle the link from 1D to 2D, we propose to rewrite the monogenic formalism in terms of *directional* RT, defined for any scalar 2D signal $\mathbf{s}(\boldsymbol{x})$ by:

$$\mathcal{R}_\theta\mathbf{s}(\boldsymbol{x}) = \cos(\theta)\Re\{\mathcal{R}\mathbf{s}(\boldsymbol{x})\}+\sin(\theta)\Im\{\mathcal{R}\mathbf{s}(\boldsymbol{x})\} \quad (12)$$

$$= |\mathcal{R}\mathbf{s}(\boldsymbol{x})|\cos(\,\theta-\arg(\mathcal{R}\mathbf{s}(\boldsymbol{x}))\,) \quad (13)$$

Here the RT is used like a pair of *steerable* filters, of which a linear combination can provide any rotation of them. The amplitude and phase turn out to be rewritable as:

$$A(\boldsymbol{x})e^{\mathbf{j}\varphi(\boldsymbol{x})} = s(\boldsymbol{x})+\mathbf{j}\mathcal{R}_{\theta(\boldsymbol{x})}s(\boldsymbol{x}) \quad (14)$$

where $\theta(\boldsymbol{x}) = \arg(\mathcal{R}s(\boldsymbol{x}))$ corresponds to the analysis of the local main direction. We already know how to deal with amplitudes and phases in the color case thanks to the elliptical model, so the last key is the color *orientation* analysis. The problem is that, at local position $\boldsymbol{x}_1$, three channels may have three different main orientations $\arg(\mathcal{R}s^{\mathsf{R}}(\boldsymbol{x}_1))$, $\arg(\mathcal{R}s^{\mathsf{G}}(\boldsymbol{x}_1))$ and $\arg(\mathcal{R}s^{\mathsf{B}}(\boldsymbol{x}_1))$.

This issue happens to be well known in differential geometry, through the *structure tensor* concept, in particular with Di Zenzo's color gradient [15, 16]. This method locally finds the orientation along which the vector signal has the maximum variation in terms of Euclidean distances. We have proposed in [17] a Riesz counterpart of it, so that we locally extract a *single* main orientation maximizing the signal's *color variation*.

Based on the fact that the RT is equal to a gradient operator combined with an isotropic low-pass filter [18, 19], a simple "replacement" by the RT provides the same quality of analysis, while bringing the connexion with the monogenic framework.

The Riesz based structure tensor is the 2 by 2 matrix defined by:

$$T = h * \sum_{\mathsf{C}\in\{\mathsf{R},\mathsf{G},\mathsf{B}\}} \begin{bmatrix} \Re\{\mathcal{R}s^{\mathsf{C}}\}^2 & \Re\{\mathcal{R}s^{\mathsf{C}}\}\Im\{\mathcal{R}s^{\mathsf{C}}\} \\ \Re\{\mathcal{R}s^{\mathsf{C}}\}\Im\{\mathcal{R}s^{\mathsf{C}}\} & \Im\{\mathcal{R}s^{\mathsf{C}}\}^2 \end{bmatrix} \quad (15)$$

where h is a smoothing filter applied on the four elements of T. The local orientation is obtained from the eigenvector tied to the largest eigenvalue of T:

$$\theta_+ = \arg(T_{11}-T_{22}+2\mathbf{j}T_{12})/2 \quad (16)$$

We here benefit from the proper analysis of *color* discontinuities thanks to a differential geometry approach.

Now that the local color orientation is given, we can define the color monogenic analysis. We propose to locally steer the color

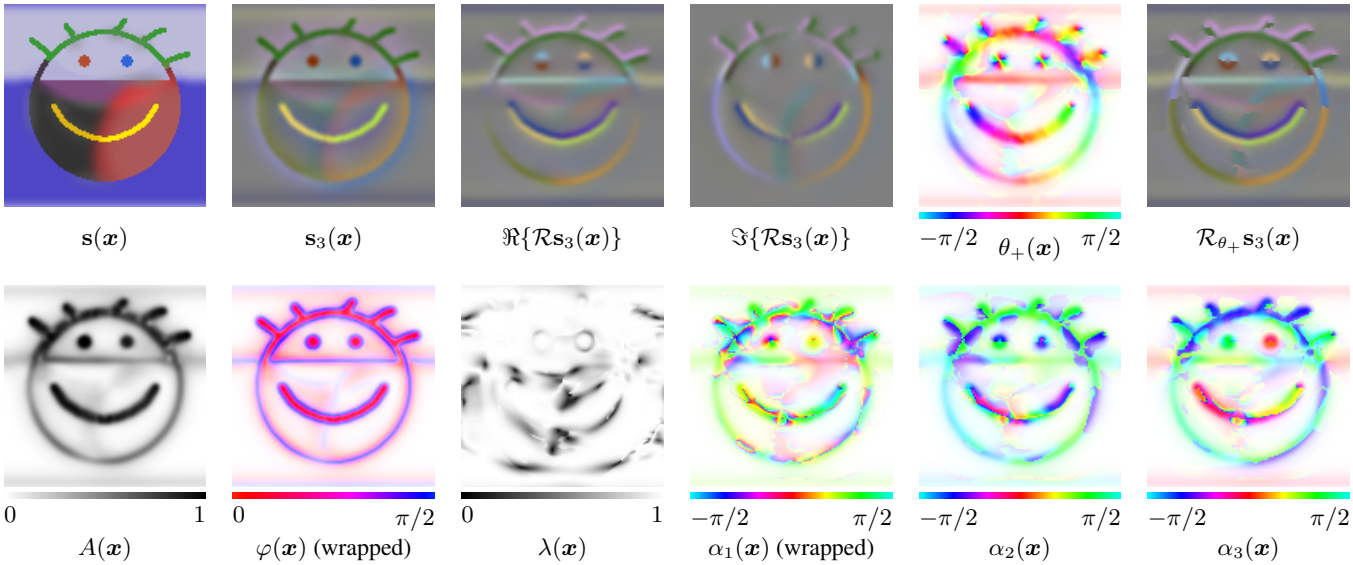

Fig. 2. Elliptical color monogenic analysis.

Riesz transform towards the same main direction θ_+ for each color channel, so that the vector amplitude-phase estimation is done coherently.

The 6 amplitude-phase parameters of eq. 5 can be defined by

$$\hat{\mathbf{a}} = \begin{bmatrix} s^{\mathsf{R}}(\boldsymbol{x}) + \mathbf{j}\mathcal{R}_{\theta_+} s^{\mathsf{R}}(\boldsymbol{x}) \\ s^{\mathsf{G}}(\boldsymbol{x}) + \mathbf{j}\mathcal{R}_{\theta_+} s^{\mathsf{G}}(\boldsymbol{x}) \\ s^{\mathsf{B}}(\boldsymbol{x}) + \mathbf{j}\mathcal{R}_{\theta_+} s^{\mathsf{B}}(\boldsymbol{x}) \end{bmatrix} = \begin{bmatrix} A^{\mathsf{R}} e^{\mathbf{j}\varphi^{\mathsf{R}}} \\ A^{\mathsf{G}} e^{\mathbf{j}\varphi^{\mathsf{G}}} \\ A^{\mathsf{B}} e^{\mathbf{j}\varphi^{\mathsf{B}}} \end{bmatrix} \tag{17}$$

and converted into ellipse parameters with formulas given in section 2, to form the *elliptical monogenic signal*:

$$s_M = [A(\boldsymbol{x})\ \varphi(\boldsymbol{x})\ \lambda(\boldsymbol{x})\ \alpha_1(\boldsymbol{x})\ \alpha_2(\boldsymbol{x})\ \alpha_3(\boldsymbol{x})] \tag{18}$$

The previous definition that we gave in [17] had the same calculus of orientation but the phase-shifted signal was limited to the Euclidean norm of the whole vector RT, instead of the more complete color directional RT proposed here. As a result, the extraction of the phase data fully benefits from the efficient ellipse parameter estimation, that properly takes into account all the rotations involved in the multidimensional space.

The vector modelling of the color 2D signal resulting in a global conversion of the data into meaningful features makes our tool a truly non-marginal method.

An illustration of the elliptical monogenic analysis is given on figure 2, from a synthetic test image featuring explicit color contours.

The first part of the calculus is illustrated on the upper row. The input image $\mathbf{s}$ is first isotropically filtered to provide $\mathbf{s}_3$. Since the result is oscillating around $(0, 0, 0)$, the graphic has been centered-normalized around the mid-grey $[128, 128, 128]$. This illustration technique is also used for the real and imaginary parts of the Riesz transform, showed next to it. The main local orientation θ_+ obtained from the Riesz structure tensor is the fifth illustration. In order to respect the circularity of the data, it is displayed as the *hue* component in the HSV color space, while the *saturation* is controlled by the amplitude A, so as to whiten irrelevant values. Here the smoothing kernel h is a gaussian filter with $\sigma = 2$. The orientation is clearly according to our perception of contours, and equally efficient on lines and edges. This is why the color directional Riesz transform $\mathcal{R}_{\theta_+}$ also performs well by phase-shifting the local oscillations from $\mathbf{s}_3$ towards the proper direction (see how the yellow line is clearly turned into a curved blue/yellow edge, with respect to x- and y- components of the RT).

Let us now observe the elliptical monogenic features on the second row.

The amplitude reveals edges as well as lines, by showing a maximum on their center, contrary to what would give a simple gradient-based contour analysis. This is due to the embedding of the *type of contour* at the core of the signal model.

As a complement, the phase φ provides the contour type information. It is here wrapped in one quadrant of the trigonometric circle, according to the symmetry of the related information [20]. We actually find $0 \pm \pi$ (red) and $\pm\pi/2$ (blue) at the centers of line- and edge- like structures respectively. This experimental result is clearly improved with respect to our previous work, in which the phase generally suffers from numerical unstability - due to the circular nature of the data being less well handled by the previous signal model.

The linearity of local color ellipse λ is near 1 almost everywhere. This means that the chosen test image contains 'simple' zero-crossing color oscillations, involving two main colors at their apogees in the color space. For example, the yellow line in test image is encoded in the subband by a variation between blue and yellow, drawing a very thin ellipse.

Finally, ellipse's position angles α_1, α_2 and α_3 are expected to convey some colorimetric information. At this stage of the work, we have no clear interpretation of it. However, these angles are necessary to the elliptical model *i.e.* they are the counterpart of the improvement for the amplitude-phase estimation - before giving any color features. Thanks to this method, the good quality of the phase estimation can now be exploited to achieve local frequency analysis from a color image.

4. LOCAL COLOR FREQUENCY

The local frequency ν is basically obtained by differentiating the local phase φ. In 2D, we have to differentiate along the main direction

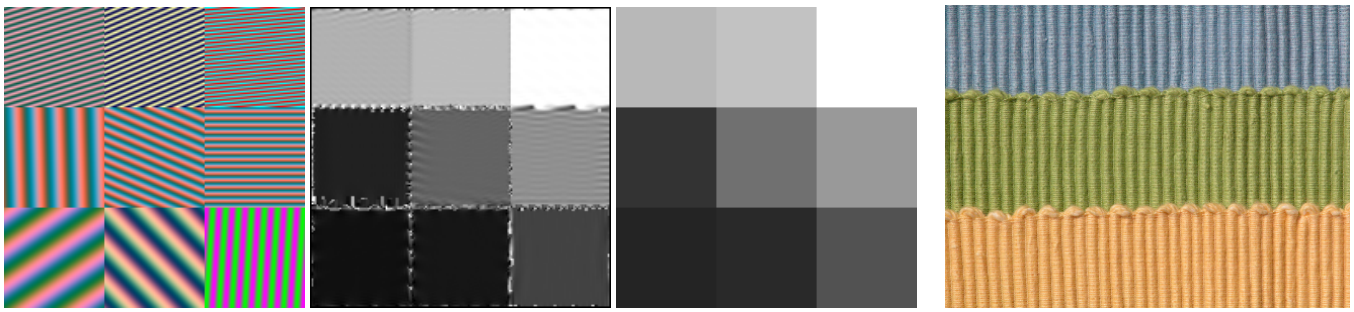

Fig. 3. Local frequency estimation. From left to right: synthetic image to analyse, estimated local frequency, theoretical correct local frequency (the grayscale is proportional to the value of $\nu \in [0; 2.5]$ rad./pixel), natural image.

of the signal, toward which the phase makes sense. This direction is explicitely given by color monogenic feature θ_+.

We apply the *central finite difference* on $\varphi(\boldsymbol{x})$. In order to steer it properly, our continuous orientation data θ_+ must be quantized so as to select the neighbour "left" φ_l and "right" φ_r samples to be compared to the local value $\varphi(\boldsymbol{x})$. We propose the following quantization formula:

$$\theta_q = (\pi/4)\,\mathtt{round}\,(\theta_+/(\pi/4)) \tag{19}$$

giving 4 possible directions: horizontal (0), vertical ($\pi/2$ and $-\pi/2$ are merged) and the two diagonals ($\pm\pi/4$).

For example, if θ_+ lies in $[-\frac{\pi}{8}; \frac{\pi}{8}]$; then the wavefront is vertical and the phase evolves horizontally. So $\varphi(x_1, x_2)$ has to be differentiated with $\varphi_l = \varphi(x_1 - 1, x_2)$ and $\varphi_r = \varphi(x_1 + 1, x_2)$.

The circularity of angle data can be handled with complex exponentials, and the local frequency defined by:

$$\nu = \left|\arg\left((\exp(\varphi_r)/\exp(\varphi_l))^{\frac{1}{2}}\right)\right| / \cos(\theta_+ - \theta_q) \tag{20}$$

The left side term compensates the bias due to orientation quantization, according to a local linear model of φ. Note that for diagonal cases ($\theta_q = \pm\pi/4$), ν must be divided by $\sqrt{2}$. There is not enough space here to give all details, this is why the reader will find the source code of the algorithm on this webpage [**?**].

The performance of this method is illustrated on figure 3. The first test is done on a synthetic image, featuring explicit local frequencies for various examples of colorimetric and geometric parameters. We expect our method to measure constant values of ν within every spatial sub-square, as shown on the third graphic. The measure is strikingly close to theoretical values, with some expectable and not damaging instability around borders. The estimation method is satisfactory for low frequencies down to $\nu = 0.35$ (period of about 18 pixels, lower-left wave) and up to $\nu = 2.5$ (≈ 2.5 pixels, upper-right wave). Efficiency is regardless of orientation and color features, which experimentally confirms the soundness of the method.

We finally test it on a natural image - fourth graphic of fig. 3. This image features a perceptually constant unique frequency, oscillating horizontally. The difficulty is that colorimetric properties are various - blue, green and yellow. We also expect measurements not to be as regular as in the synthetic case, in particular due to richer frequency content, and randomness of real data. This is why a prior frequency band selection has been done with an isotropic filter, and the estimated $\nu(\boldsymbol{x})$ has been regularized by a 11×11 median filtering.

The figure 4 below shows the estimated frequency as a 3D mesh, together with a histogram of the measured $\nu(\boldsymbol{x})$. Apart from a mild random variation due to the original image itself, we can see that ν still lies within a small interval around $\nu = 0.6$ rad./pixel. This value corresponds to a period of around 10 pixels, which is well according to the visible pattern in this image, actually of this kind of periodicity. To our knowledge, no existing work deals with local

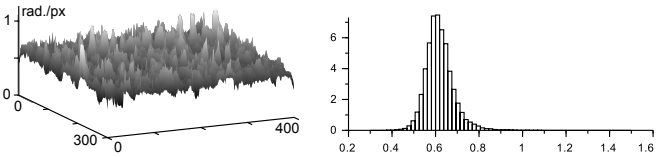

Fig. 4. Mesh and histogram of estimated local frequency from the natural image shown in figure 3.

frequency of color images. This experiment shows that our elliptical monogenic representation actually provides sound data, according to a oscillatory model in the spirit of the classical Fourier analysis, with a intuitive extension of the amplitude and phase concept.

We are currently working on integrating this tool into a reversible filterbank algorithm, so as to carry out new color wavelet transforms and apply them to image enhancement and compression.

5. CONCLUSION

We have defined a new color monogenic representation providing amplitude, phase, orientation and colorimetric local features. The building blocks are the elliptical model, the directional Riesz transform and the structure tensor. The construction is driven by the physical meaning of the data, ending up with an easily usable local phase, thanks to a truly non-marginal definition. This phase is numerically differentiated to carry out the local frequency: a new concept for color images. The algorithm proves to be efficients on synthetic and natural images. We have seen that the different pieces of information are well separated and independent from each other. This could be the basis for a new generation of SIFT-like detectors. Our current work investigates the wavelet counterpart of this framework.

R. Soulard is partially supported by Crescen2o.

6. REFERENCES

[1] Michael Felsberg, "Low-level image processing with the structure multivector," *Thesis*, 2002.

[2] Lin Zhang, Lei Zhang, Zhenhua Guo, and David Zhang, "Monogenic-lbp: A new approach for rotation invariant texture

classification," in *Proc. IEEE Int'l Conf. on Image Processing*, 2010, pp. 2677–2680.

[3] Tanguy Maltaverne, Philippe Delachartre, and Adrian Basarab, "Motion estimation using the monogenic signal applied to ultrasound elastography," in *Proc. IEEE Eng. Med. Biol. Soc. Conf. (EMBC'10)*, Buenos Aires, Argentina, 2010, pp. 33–36.

[4] Jinjun Li, Hong Zhao, Chengying Shi, and Xiang Zhou, "A multi-model stereo similarity function based on monogenic signal analysis in poisson scale space," *Math. Prob. Eng.*, 2011.

[5] A. Belaid, D. Boukerroui, Y. Maingourd, and J. F. Lerallut, "Phase-based level set segmentation of ultrasound images," *Trans. Info. Tech. Biomed.*, vol. 15, no. 1, pp. 138–147, Jan. 2011.

[6] Niranjan Joshi, Sarah Bond, and Michael Brady, "The segmentation of colorectal MRI images," *Medical Image Analysis*, vol. 14, no. 4, pp. 494–509, 2010.

[7] K. G. Larkin, D. Bone, and M. A. Oldfield, "Natural demodulation of two-dimensional fringe patterns: I. general background to the spiral phase quadrature transform," *J. Opt. Soc. Am.*, vol. 18 (8), pp. 1862–1870, 2001.

[8] Misac N. Nabighian, "Toward a three-dimensional automatic interpretation of potential field data via generalized Hilbert transforms: Fundamental relations 780786.," *Geophysics*, vol. 49, no. 6, 1984.

[9] Alan Conrad Bovik, *Handbook of Image and Video Processing*, Academic Press, May 2000.

[10] Guillaume Demarcq, Laurent Mascarilla, Michel Berthier, and Pierre Courtellemont, "The color monogenic signal: Application to color edge detection and color optical flow.," *J. Math. Im. Vis. (JMIV)*, vol. 40, no. 3, pp. 269–284, 2011.

[11] Raphaël Soulard and Philippe Carré, "Color monogenic wavelets for image analysis," in *Proc. IEEE Int'l Conf. on Image Processing*, Brussels, Belgium, Sep. 2011, pp. 277–280.

[12] Thomas Batard and M. Berthier, "Spinor fourier transform for image processing," *IEEE Journal of Selected Topics in Signal Processing (Special Issue on Differential Geometry in Signal Processing) IEEE JSTSP*, vol. 7, no. 4, pp. 605–613, 2013.

[13] Fred Brackx, N. De Schepper, and F. Sommen, "The two-dimensional clifford-fourier transform," *J. Math. Imaging Vision*, vol. 26, no. 1-2, pp. 5–18, 2006.

[14] J. M. Lilly, "Modulated oscillations in three dimensions," *IEEE Trans. Signal Process.*, vol. 59, no. 12, pp. 5930–5943, 2011.

[15] Silviano Di Zenzo, "A note on the gradient of a multi-image," *Computer Vision, Graphics, and Image Processing*, vol. 33, no. 1, pp. 116–125, 1986.

[16] Guillermo Sapiro and Dario L. Ringach, "Anisotropic diffusion of multivalued images with applications to color filtering," *IEEE Trans. Image Process.*, vol. 5, no. 11, pp. 1582–1586, 1996.

[17] Raphaël Soulard, Philippe Carré, and Christine Fernandez-Maloigne, "Vector extension of monogenic wavelets for geometric representation of color images," *IEEE Trans. Image Process.*, vol. 22, no. 3, pp. 1070–1083, Mar. 2013.

[18] Ullrich Köthe and Michael Felsberg, "Riesz-transforms versus derivatives: On the relationship between the boundary tensor and the energy tensor," in *Proc. Scale-Space, LNCS 3459*, J. Weickert R. Kimmel, N. Sochen, Ed. 2005, pp. 179–191, Springer.

[19] Michael Unser, Daniel Sage, and Dimitri Van De Ville, "Multiresolution monogenic signal analysis using the riesz-laplace wavelet transform," *IEEE Trans. Image Process.*, vol. 18, no. 11, pp. 2402–2418, 2009.

[20] Michael Felsberg and Gerald Sommer, "The monogenic signal," *IEEE Trans. Signal Process.*, vol. 49, no. 12, pp. 3136–3144, 2001.